

CDC-42 encodes dynamically stable asymmetries in the *C. elegans* zygote via an incoherent feed-forward loop

Ondrej Maxian, Cassandra Azeredo-Tseng, . . . , and Edwin Munro

April 20, 2024

Introduction

Cell polarity is essential for many aspects of organismal development and physiology, including stem cell dynamics, directional cell migration, and asymmetric cell division (Dewey et al., 2015; Goldstein and Macara, 2007; Ierushalmi and Keren, 2021; Maître et al., 2016). For most cells, the first step in polarization involves a symmetry-breaking response to a transient localized cue that creates asymmetric distributions of specific molecules or molecular activities. The mechanisms that underlie cellular symmetry-breaking have been extensively explored (Li and Bowerman, 2010), but mechanisms that maintain polarity as a dynamically stable state with a fixed boundary position have only recently come under scrutiny (Sailer et al., 2015; Gross et al., 2019).

On a large scale, a cell’s polarity state is encoded by asymmetric distributions of protein molecules, which are shaped by smaller-scale processes like binding, diffusion, and active transport. In *C. elegans*, polarity is encoded by the distribution of two distinct groups of (highly conserved) polarity proteins: anterior PARs (aPARs), which include the scaffold PAR-3, adaptor PAR-6, atypical kinase PKC-3, and GTPase CDC-42, and posterior PARs (pPARs), which include the RING-domain containing protein PAR-2 (Bland et al., 2023), kinase PAR-1, tumor suppressor LGL-1, and CDC-42 GAP CHIN-1 (Lang and Munro, 2017).

Wild-type embryos polarize in two distinct phases termed “establishment” and “maintenance” (Cuenca et al., 2003). The mechanisms that underlie symmetry-breaking during polarity establishment have been well-studied (Cowan and Hyman, 2007; Munro and Bowerman, 2009). Near the end of meiosis, PAR-3, PAR-6 and PKC-3 are uniformly distributed at the cortex, where they prevent cortical association of PAR-1, PAR-2 and LGL-1 (Schonegg and Hyman, 2006; ?). One mode of symmetry-breaking involves the local inhibition of actomyosin contractility near the sperm MTOC,

which triggers cortical flows that transport F-actin, myosin II, PAR-3/PAR-6/PKC-3, and other cortically associated factors towards the anterior pole, resulting in their mutual restriction to an anterior cap (Munro et al., 2004; Rodriguez et al., 2017). Posterior depletion of PAR-3/PAR-6/PKC-3 then allows PAR-1, PAR-2 and LGL-1 to associate with a complementary posterior domain. Actomyosin contractility and cortical flow during polarity establishment require the small GTPase Rho-1 (Schonegg and Hyman, 2006; Motegi and Sugimoto, 2006), and in fact the sperm cue acts via Aurora A kinase (AIR-1) to locally inhibit Rho through the Rho GEF Ect-2 (Motegi and Sugimoto, 2006; Tse et al., 2012; Longhini and Glotzer, 2022; Kapoor and Kotak, 2019). A second mode of symmetry-breaking has also been described in which sperm astral microtubules promote local association of Par-2 with the posterior cortex (Motegi et al., 2011).

While the mechanisms that break symmetry are by now well understood, it remains unclear what *stops* symmetry breaking. If the system is programmed to amplify an initial polarizing cue, what sets the limit of amplification? The by now standard mechanism is that anterior (CDC-42/PAR-3/PAR-6/PKC-3) and posterior proteins (PAR-1/PAR-2/LGL-1) form a bistable reaction diffusion system by competing for residence at the cortex/plasma membrane such that one or the other but not both win locally. Theoretical studies suggest that in principle such a mechanism could stabilize the AP boundary after establishment phase cortical flows cease, or in embryos that lack cortical actin or myosin (Mori et al., 2008; Dawes and Munro, 2011; Goehring et al., 2011; Lang et al., 2023). These mechanisms by themselves cannot, however, shift the boundary on realistic timescales (Lang et al., 2023), which is why flow is required.

In the presence of flow, it is still unknown what sets a limit to boundary progression. Recent work showed that, assuming an intrinsic self limit to contractility, the boundary can be pinned, with the position set by total amount of each PAR protein (Gross et al., 2019; Goehring et al., 2011). But the self-limiting nature of the flow remains a mystery. In wild type embryos, myosin accumulates at the anterior in a cap that takes up about 50% of the embryo, and myosin flows from the posterior half of the embryo into the anterior cap. Despite the flow of myosin and the consequent A/P asymmetry in contractility, the cap maintains a fixed size (it does not contract), and the flow profile in the anterior is roughly zero (Sailer et al., 2015). Moreover, ectopic accumulation of Myosin II during maintenance in PAR-2 mutants is associated with abnormal posterior-directed cortical flows and rapid redistribution of Par proteins (Munro et al., 2004), suggesting that the distribution of myosin, in addition to the PAR proteins, guides the steady state.

While we will show that the self-limiting nature of contractility applies in both establishment

and maintenance phase, our focus in particular will be on maintenance, which requires CDC-42 to maintain asymmetries set up during establishment (Kay and Hunter, 2001; Gotta et al., 2001; Aceto et al., 2006; Schonegg and Hyman, 2006; Motegi and Sugimoto, 2006). GFP-tagged CDC-42 becomes anteriorly enriched during polarity establishment, and studies with a GFP-tagged biosensor suggest that the active (GTP-bound) form of CDC-42 may be similarly enriched during maintenance phase (Kumfer et al., 2010). Binding of CDC-42 to the conserved semi-Crib domain of PAR-6 is required for cortical association of PAR-6/PKC-3 during maintenance (Aceto et al., 2006), and PKC-3 is in an active state only when bound to CDC-42 (Sailer et al., 2015; Lang and Munro, 2017; Rodriguez et al., 2017). CDC-42 also acts through MRCK-1, a *C. elegans* orthologue of the mammalian Myotonia Dystrophy-related CDC-42-binding kinase MRCK, to promote asymmetric cortical recruitment of myosin II (Kumfer et al., 2010). There is also evidence that CDC-42 promotes asymmetric enrichment of F-actin during maintenance phase (REF?), but the underlying mechanism remains poorly understood. More generally, it remains unclear how these distinct outputs of CDC-42 are integrated to dynamically stabilize the AP boundary at a fixed axial position and limit contractility.

In this study, we combine experiments and theoretical modeling to show that boundary progression can be stalled when distinct outputs of CDC-42 have different effects on contractility. By extending both establishment and maintenance phases, we show that the boundary position is in fact stable, regardless of the cell cycle phase. We then demonstrate, through experiments with a temperature sensitive ECT-2 gene (Zonies et al., 2010), that the steady state observed at the end of maintenance phase can be reproduced even when establishment fails through a maintenance-phase rescue process, revealing that maintenance phase biochemistry encodes a dynamically stable attractive state. To understand how the PAR protein circuit (which involves CDC-42) interacts with myosin contractility to limit the extent of contractility, we introduce a continuum model. Without a self-limiting character to the flow, the boundary either contracts all the way to the end of the embryo, or slowly moves to the embryo interior over a timescale an order of magnitude longer than maintenance phase. To find the missing model component, we return to experiments, which demonstrate that branched actin in the anterior acts to reduce tension and prevent excessive contraction, similar to behavior observed previously in other systems (Muresan et al., 2022; Yang et al., 2012). Our model reveals that adding a threshold of CDC-42, above which branched actin is produced, is sufficient to reproduce the initial and latter stages of rescue, with the caveat that additional assumptions about branched actin are required to reproduce all experimental observations.

Results

Establishment and maintenance phase contractility are governed by unique biochemical systems

As a first step to examining the role of CDC-42 in regulating contractility, we sought to distinguish the phases of the cell cycle in terms of the upstream protein which ultimately regulates myosin. We began by imaging wild-type embryos expressing non-muscle myosin II fused to GFP (NMY-II::GFP), as well as embryos expressing PAR-6::GFP. At pseudo-cleavage and prior to the onset of centration (Fig. 1a), myosin exhibited pulsatile dynamics, with large foci appearing and disappearing over time, and PAR-6 was enriched in clusters on the anterior cortex (Fig. 1b). By nuclear envelope breakdown, both myosin and PAR-6 had transitioned to diffuse, smaller clusters enriched on the anterior cortex. Pulsatile myosin activity during establishment phase has previously been shown to involve rho-mediated contractility (Michaux et al., 2018; Michaud et al., 2022; Yao et al., 2022), while the diffuse myosin clusters have been previously linked to CDC-42 (Motegi and Sugimoto, 2006). Likewise, previous reports (Motegi and Sugimoto, 2006; Rodriguez et al., 2017) have shown that the diffuse PAR-6 clusters are correlated with binding to CDC-42, which activates PKC-3, while the punctate clusters are linked to PAR-3. We therefore conclude that Rho-1 mediates contractility during polarity establishment phase, while CDC-42 controls both contractility and PAR polarity during maintenance phase. The coupling of biochemistry and contractility through CDC-42 makes maintenance unique relative to establishment.

To understand the transition from establishment to maintenance, we depleted embryos of PRI-1 via RNAi. Depletion of PRI-1 prevented DNA replication and stalled cells in late establishment phase (Fig. 1c). In particular, we found a typical delay time of about eight minutes from pronuclear meeting to centration onset, relative to wild type embryos (Fig. 1d). The delay in centration onset also correlated with a delay in pseudo-cleavage relaxation (middle kymographs in Fig. 1c), and prolonged flows from the posterior into the psuedo-cleavage region (rightmost kymographs in Fig. 1c). Regardless of the embryo treatment, we found a strong correlation between three events: centration onset, psuedo-cleavage relaxation, and the myosin transition from punctate to diffuse. We conclude that these events mark the transition from establishment to maintenance, and especially to the regime of CDC-42-mediated contractility. While this regime is our interest here, it is noteworthy that embryos in late establishment phase (especially PRI-1 depleted embryos) exhibit a stable A/P myosin asymmetry characterized by persistent anterior-directed flow, similar

to previous observations for maintenance phase. We return to this point in the discussion.

The steady state of maintenance phase is a stable boundary with persistent anterior-directed flow

A recent examination of polarity establishment linked the end of establishment phase with a vanishing flow profile and a stable A/P asymmetry coming from mutual exclusion of PAR proteins (Gross et al., 2019). Yet, embryos in late-maintenance phase exhibit a steady pattern of anterior-directed cortical flow with an asymmetric myosin profile (Sailer et al., 2015, Fig. 2). We consequently wondered which of the two pictures represents the true “steady state” of maintenance phase.

To probe whether the previously-observed myosin intensity and patterns of flow in late maintenance phase are truly steady states, we extended maintenance phase by depleting wild-type embryos of the cell cycle regulator CDK-1. Marking maintenance phase as the period between pseudocleavage relaxation and anaphase onset, we obtained a window of roughly 8–10 minutes per cell, in which we characterized the myosin intensity and flow speeds. Later stages of the extended maintenance phase showed a relatively stable position of the myosin boundary (it in fact expands towards the posterior slightly) and a persistent anterior-directed flow which tends to achieve a maximum (magnitude) just posterior of the peak myosin location (Fig. 2A). However, because the myosin intensity and flow speeds in CDK-1 (RNAi) never resemble those of wild-type, it is clear that interfering with CDK-1 affects more than just the cell cycle, and it is impossible to say concretely that the specific flow and myosin profiles in late maintenance are “steady.” Nevertheless, we can conclude that an asymmetric myosin profile and persistent anterior-directed flow do not lead to further contraction of the boundary when maintenance is extended.

The maintenance phase steady state is unique and attractive in the presence of MRCK

We next wanted to determine if the boundary position in maintenance phase is unique, or if it is a consequence of the dynamics of establishment. Previous studies in *ect-2* mutants (which fail to establish polarity due to lack of rho activity) have reported a delayed symmetry breaking (Zonies et al., 2010; Tse et al., 2012), but have not directly explained this as a maintenance-phase phenomenon, nor studied how the boundary position and flow profile change relative to normal maintenance phase.

To probe these dynamics further, we systematically imaged symmetry breaking in temperature-sensitive *ect-2* mutants, marking the beginning of maintenance phase via the transition of myosin from large to small clusters (since there is no pseudocleavage), and the end of maintenance phase as the onset of embryo rotation prior to cytokinesis. As described in previous reports (Zonies et al., 2010), embryos exhibited symmetry breaking that we refer to as “maintenance phase rescue,” since it occurred only when myosin was distributed in diffuse clusters. During rescue, myosin and anterior PAR proteins segregated into an anterior domain of the same size as in wild-type embryos. At the end of rescue, the pattern of flow was characterized by a stronger flow in the posterior half of the cell into a stall point at the edge of the anterior cap, as in wild type embryos (Fig. 2B). Embryos depleted of the kinase MRCK, which acts downstream of CDC-42 to activate myosin, failed to rescue polarity in maintenance phase, as neither the anterior domain nor myosin domain contracted towards the anterior (Fig. 2B).

Having characterized maintenance phase dynamics when establishment phase is either totally effective or totally ineffective, we wondered if having partial polarity establishment would lead to partial polarity rescue. To accomplish this, we depleted embryos of NOP-1, a protein which partially mediates contractility by activating rho (Tse et al., 2012). Exposing embryos to varying degrees of NOP-1 (RNAi) led to varying boundary positions at the end of establishment phase. Upon the transition to maintenance phase, cortical flows were initiated, and the boundaries in each of the cells converged to the same approximate position at roughly 60% embryo length (Fig. 2C). By contrast, in the absence of MRCK, the A/P boundary stayed in the same position throughout maintenance phase, and no cortical flows were initiated. We conclude that maintenance phase encodes an attractive steady state with a unique boundary position and flow pattern. When establishment is defective, CDC-42/MRCK-mediated cortical flows during maintenance phase rescue the correct boundary position.

Existing models cannot explain the dynamics of maintenance phase rescue

We now explore whether a mathematical model, informed by existing knowledge of maintenance phase, could explain its tendency to correct errors from establishment. At first glance, it appears that the phenomenon of maintenance-phase rescue could be a consequence of an instability in the underlying myosin dynamics. In the SI, we consider this possibility by performing linear stability analysis of a simple myosin model informed by our experimental data (Mayer et al., 2010; Bois et al., 2011). The stability analysis shows that the dynamics are unstable when the flow carries

myosin molecules a distance larger than the hydrodynamic lengthscale, which is the typical length a local disturbance propagates through flows (Mayer et al., 2010). For realistic lifetimes on the order 5–20 s, the minimum flow speed to generate instability is about 40 $\mu\text{m}/\text{min}$, which is much faster than ever observed in maintenance phase. Thus the dynamics of maintenance phase rescue are not due to myosin instabilities.

Because the dynamics of myosin alone are insufficient to generate instability, PAR proteins must be essential for rescue to occur, as was previously shown in the case of PAR-2 (Zonies et al., 2010). We consequently introduce a model of maintenance phase biochemistry based on previously-characterized interactions (Fig. 3A), (Lang and Munro, 2017). On the anterior side, we have three distinct protein species: PAR-3, CDC-42, and PAR-6/PKC-3, each of which has a separate function. The posterior PARs (PAR-2, PAR-1, and CHIN-1) can be lumped into one species (denoted by P), which antagonizes both PAR-3 and CDC-42. A schematic diagram is given in Fig. 3A, and equations which describe the circuit are given in the SI. In brief, PAR-3 is locally bistable dynamics because of oligomerization and positive feedback Lang et al. (2023). The enriched zone of PAR-3 sets up a gradient of PAR-6/PKC-3, which inhibits all of the posterior PAR proteins. The posterior PARs then inhibit CDC-42 (directly through CHIN-1 and indirectly through PAR-2) (Munro et al., 2004; Sailer et al., 2015).

In the absence of contractility, our model shows that the maintenance phase circuit has a unique boundary position, where the PAR-3 boundary sits at about 50% embryo length (Fig. 3B). Under normal circumstances, where the boundary begins at 50% embryo length (the end of establishment phase), the boundary rapidly adjusts to its unique position in under ten minutes. By contrast, under rescue conditions, where there is local loading of pPARs in the posterior-most 10% of the embryo, the boundary slowly corrects, taking about an hour to reach steady state. The steady state here is reached through a wave-pinning mechanism (Mori et al., 2008; Goehring et al., 2011), where the boundary stops moving when reaction and diffusion fluxes (both of which depend on the cytoplasmic protein concentration) come into balance. The change in protein concentration occurs through unbinding, which for most proteins occurs on the timescale of hundreds of seconds (Robin et al., 2014), thus explaining the slow dynamics. Our model therefore confirms the experimental result that rescue is impossible without flows.

To model contractility, we make CDC-42 a promoter of myosin at the cortex, and cortical tension directly proportional to myosin (blue parts in Fig. 3A, see SI for equations). Flow occurs in the direction of gradients in cortical tension, and all proteins on the cortex are advected with

the local cortical velocity (Illukkumbura et al., 2023). With contractility, simulations under rescue conditions reproduce the initial stages of rescue (Fig. 3C), where an initially peaked profile of pPARs invades the anterior domain, concentrating aPARs in the middle and thereby increasing the concentration of pPARs in the posterior. As a result of this, CDC-42 gets inhibited in the posterior, which gives a gradient of myosin from posterior to anterior. The gradient of myosin generates a flow which further compacts the anterior domain. The timescale of this compaction is much faster than without flows, and indeed occurs on a timescale of minutes and not hours.

While the model reproduces the initial stages of the rescue process, there is no mechanism in it to halt the advancing myosin front. Indeed, without flows the reaction-diffusion mechanism relied on aPARs becoming enriched in the anterior to eventually out-compete pPARs and stall the boundary. But when enrichment of aPARs also enriches myosin, flow speeds also increase, and the additional advective flux of pPARs overwhelms the increasing reactive flux, resulting in an ever-contracting boundary with ever-increasing flows and pPARs becoming uniformly enriched.

In order to properly reproduce rescue, the model suggests a need for a local inhibitor of contractility. If an additional agent can inhibit contractility without inhibiting other aPAR proteins, the reactive flux and advective flux would decouple, and the reaction-diffusion mechanism can stall the boundary. We return next to experiments to find such an inhibitor.

Branched actin prevents hypercontractility and is necessary for successful rescue

Previous studies in other systems (Yang et al., 2012; Muresan et al., 2022) have suggested that branched actin networks could constrain myosin mini-filament motion, thereby inhibiting contractility. To see if this mechanism could also be at work in the *C. elegans* zygote, we first compared F-actin organization in fixed, phalloidin-stained wild type and CDC-42-depleted embryos (Fig. 4A). In all embryos, a loose network of long filaments or filament bundles extended throughout the posterior cortex. Numerous bright puncta (hereon mini-comets) were enriched within an anterior cap, and a denser meshwork of filaments was also enriched within the anterior cap in a cortical layer superficial to the mini-comets.

Depletion of CDC-42 resulted in nearly complete loss of both mini-comets and the dense anterior meshwork, leaving a more uniform network of longer filaments/bundles (Fig. 4A) similar to that seen at the posterior cortex in the wild type. Thus, CDC-42 is required for localized assembly of a specific subset of filaments during maintenance. In other cell types, CDC-42 binds WASP family proteins to activate ARP2/3-dependent branched actin assembly (Pollitt and Insall, 2009).

Consistent with this, depleting embryos of the essential ARP2/3 subunit ARX-2 caused a complete loss of both F-actin mini-comets and the dense anterior meshwork during maintenance, leaving the loose network of filaments similar to that seen at the posterior cortex in the wild type. Similarly, depleting embryos of the single *C. elegans* WASP homologue WSP-1 resulted in a severe reduction of the dense anterior mesh, although mini-comets remained highly enriched in the anterior cap (Fig. 4A). We conclude that CDC-42, acting through WASP, promotes the production of branched actin structures in the anterior.

To determine the effect of branched actin structures on contractility, we first returned to our model to see if there is a contractile asymmetry across the A/P boundary. Using velocity data from late maintenance phase in wild type embryos, we used a simple active fluid model (Mayer et al., 2010) to extract a profile of stress, which we compared directly to the measured myosin intensity on the cortex (Fig. 4B). While there was perfect agreement between stress and myosin on the posterior, in the anterior there was a noticeable mismatch, with the gradient in stress being smaller predicted from the myosin profile. The reduction in anterior stress, combined with localization of branched actin in the anterior, suggests that branched actin might be responsible for inhibiting contractility there.

To test this hypothesis, we performed live imaging of myosin dynamics in embryos depleted of arx-2. Unlike in wild type embryos, which formed a stable cap that remained steady in maintenance phase, embryos depleted of arx-2 exhibited hypercontractility, with caps that tended to progress towards the anterior pole during maintenance phase (Fig. 4C). We tracked the myosin intensity during the three minutes prior to cytokinesis, finding a maximum intensity which progressively moves towards the anterior pole and grows over time (blue lines in Fig. 4D), in contrast to wild-type embryos, where the maximum myosin intensity retains a fixed position in the last three minutes of maintenance phase (red lines in Fig. 4D). Similar to the myosin intensity, we found the flow profile in arx-2 (RNAi) embryos did not display a stall point near the anterior cap, but instead exhibited persistent anterior-directed flows throughout the whole embryo length (Fig. 4D). **We found a similar phenotype in WASP (RNAi) embryos.**

Our observations of the flow profile in arx-2 (RNAi) embryos were somewhat confounded by their tendency to exhibit unstable rotation, leading to large bulk flows that were not aligned with the A/P direction. We hypothesized that these rotations could be caused by microtubule forces (from the mitotic spindle) pulling on the smaller anterior cap, which can no longer effectively resist them. Consistent with this, treating arx-2 (RNAi) embryos with nocodazole, a drug which depolymerizes

microtubules, removed the large-scale rotations and led to more consistent measurements of flow. The resulting myosin intensities and flow profiles (Fig. 4D) were almost identical to those without nocodazole treatment, in that they exhibited a myosin peak which continuously shifted to the anterior, and a flow which was anterior-directed and on the order 2–4 $\mu\text{m}/\text{min}$ across the whole embryo length.

The phenotype we observed in embryos depleted of branched actin was consistent with our previous model of maintenance phase without inhibition (Fig. 3C), in that the flow was persistently anterior directed and the myosin profile consistently shifted towards the anterior. Indeed, repeating our previous experiment (Fig. 4B), in which we use the velocity profile during the last minute of maintenance phase to extract a stress and compare to the myosin profile ([which embryos](#)), showed perfect agreement between myosin and stress across the entire embryo length in arx-2 (RNAi) embryos. Thus, in wild type embryos branched actin must act in the anterior to inhibit contractility.

The dynamics of rescue suggest an activation threshold for branched actin

To further inform our model of branched actin, we looked at the dynamics of maintenance-phase rescue with and without branched actin. We first tested the effect of branched actin knockdown during maintenance phase rescue by depleting ect-2 (ts) embryos of arx-2. Unlike in normal rescue, where contraction of the anterior domain suddenly stalled, in embryos depleted of arx-2 the anterior domain appeared to contract at a constant rate until cytokinesis (Fig. 5A). The sudden stalling of the boundary in the presence of branched actin suggests a sudden production of branched actin on the anterior, which begins at a mid-point in the rescue process.

To further probe this idea, we systematically imaged the myosin intensities and flow profiles during rescue, with the average profiles every 30 seconds of rescue shown in Fig. 5B. We observed two distinct phases of rescue: in the first phase, the myosin intensity slightly increased, and the peak shifted towards the anterior. Meanwhile, flow speeds increased, with the peak in flow also shifting towards the anterior. After around three minutes, we observed a sudden decrease in flow speeds so that the flow profile matched the typical profile from late maintenance phase in wild type embryos (black line in Fig. 5B), which then stalled the myosin boundary at a fixed point near the typical wild-type boundary. To understand further the temporal dynamics of rescue, we plotted the maximum myosin intensity and flow speeds, as well as the position of the maxima, over time (Fig. 5C). This revealed the order of events in the stalling of rescue: first, the flow speed suddenly decreased, which led to the stalling of the myosin boundary, and finally the stalling of the flow

boundary. All of this occurred *without* significant changes in the myosin profile (in particular the maximum myosin intensity). Thus, if branched actin is activated in the anterior midway through rescue, its role is to inhibit flow speeds, and not directly inhibit myosin. This observation forms the basis of our model in the next section.

Incorporating branched actin into existing models correctly reproduces rescue dynamics

To model branched actin, we work off the following two important observations from our maintenance-phase rescue experiments: first, the pinning of the myosin domain and drop in velocity happen quite abruptly, and second, the rapid drop in velocity is *not* accompanied by strong changes in the myosin concentration profile (Fig. ??). These observations together suggest that there is an ultra-sensitive dependence of contractility (not myosin concentration) on branched actin. As rescue progresses, branched actin becomes active on the anterior, providing a “brake” which slows down contractility and progression of the boundary.

To translate our hypothesis into our model, we make the following assumptions,

1. To activate branched actin, we assume a threshold of CDC-42 above which branched actin is created. The threshold is reached roughly when the A/P boundary reaches the middle of the cell.
2. Branched actin assembly is autocatalytic, since new branches become sites for additional branches.
3. Branched actin unbinds from the cortex with characteristic rate k_R^{off} (about 8 s lifetime).
4. While branched actin does not diffuse in the cortex, polymerization of actin leads to a spreading out of the branched network, and so we include nonzero diffusivity.
5. Branched actin inhibits contractility.

The first four assumptions lead to the advection-diffusion-reaction equation for branched actin given in the SI. For the fifth assumption, we postulate a simple relationship for how branched actin impacts contractile stress, given in the SI.

The dynamics of rescue in this case are shown in Fig. ???. In the early stages of rescue, we see a concentration of myosin and CDC-42 into an interior peak which grows over time. Once the

concentration of CDC-42 at the peak exceeds the threshold $C_R = 0.25$, branched actin is produced. This causes an immediate drop in contractility within the peak (see the active stress profile at intermediate times), which leads to a leveling out of the anterior profiles of CDC-42 and myosin (weaker flows in the anterior allow CDC-42 to diffuse over). Following this, branched actin builds up on the anterior. The boundary stops moving when the tension on the anterior balances the tension on the posterior, leaving an intermediate zone of contractility at around 60% embryo length.

A necessary feature of our simulations is the threshold dependence of branched actin production on CDC-42 activity.

Discussion

We note a distinction here between maintenance and establishment phase. In the latter, instabilities in the dynamics of rho combine with delayed negative feedback to yield pulsatile dynamics (Nishikawa et al., 2017; Michaux et al., 2018; Michaud et al., 2022). The connection between these pulsatile dynamics and the large-scale flows that establish polarity is still unknown.

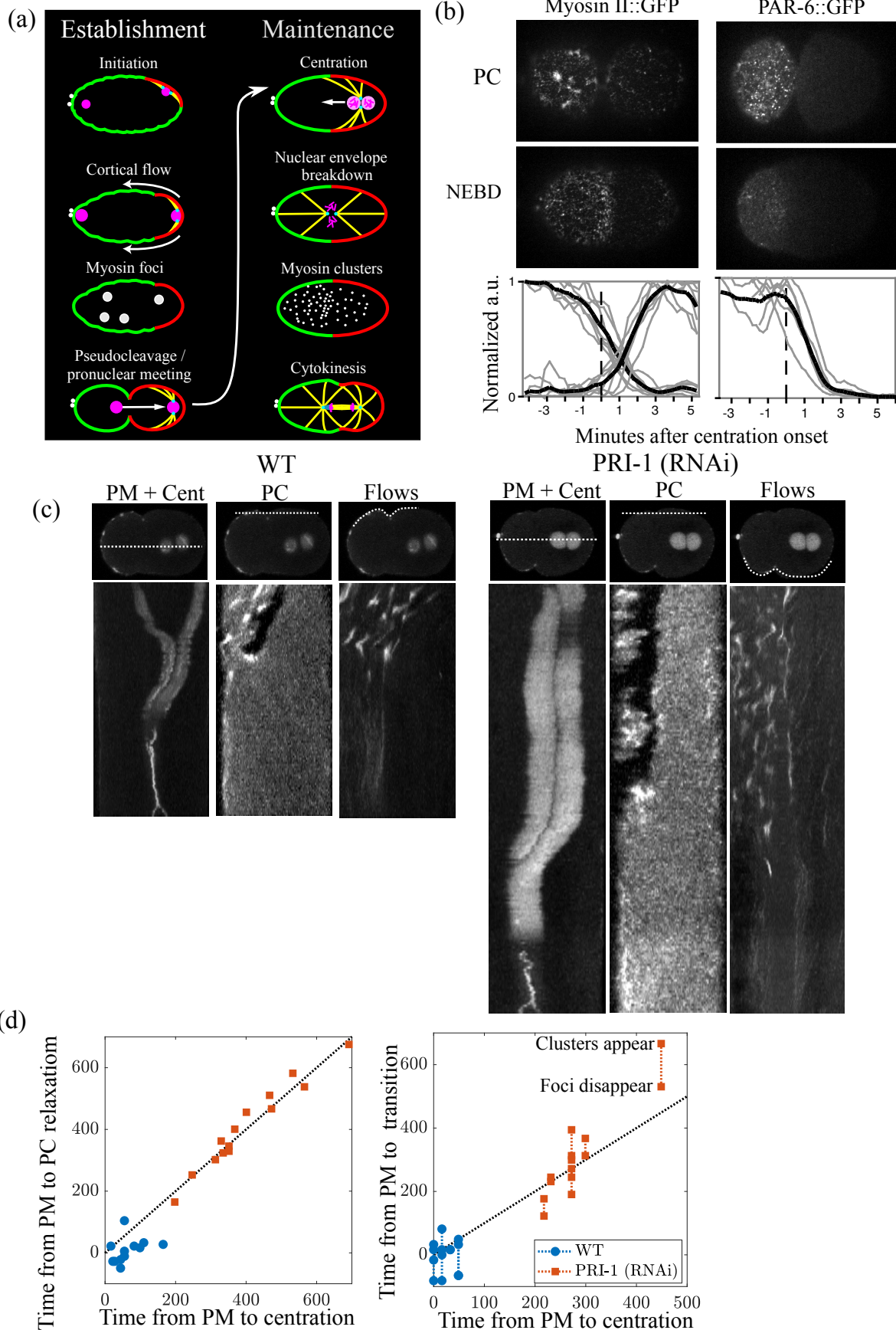


Figure 1: Cell cycle progression controls a regime change from rho-dependent to CDC-42-dependent contractility. (a) Overview of dynamics during establishment and maintenance phase, including key events in the cell cycle. (b) Distributions of non-muscle-myosin II (NMY-2::GFP; left panels) GFP::PAR-6 (right panels) in wild-type embryos at/near the end of pseudocleavage (top panels) or nuclear envelope breakdown (bottom panels). Graphs show the normalized intensity of myosin foci and clusters (left), or PAR-6 clusters (right) over time relative to centration onset. (c) Kymographs showing the correlation between pronuclear meeting and centration (left), pseudocleavage relaxation (middle), and flow into the pseudocleavage (right) in wild type (left) and PRI-1 (RNAi) embryos. (d) Correlation between centration and pseudocleavage relaxation (left) and centration and myosin transitions (right) in wild-type (blue circles) and PRI-1 (RNAi) embryos (red squares). **First draft complete.**

Figure 2: Maintenance phase biochemistry encodes a stable, attractive steady state with a unique boundary position. (a) CDK-1, (b) ect-2 ts, (c) Charlie’s data.

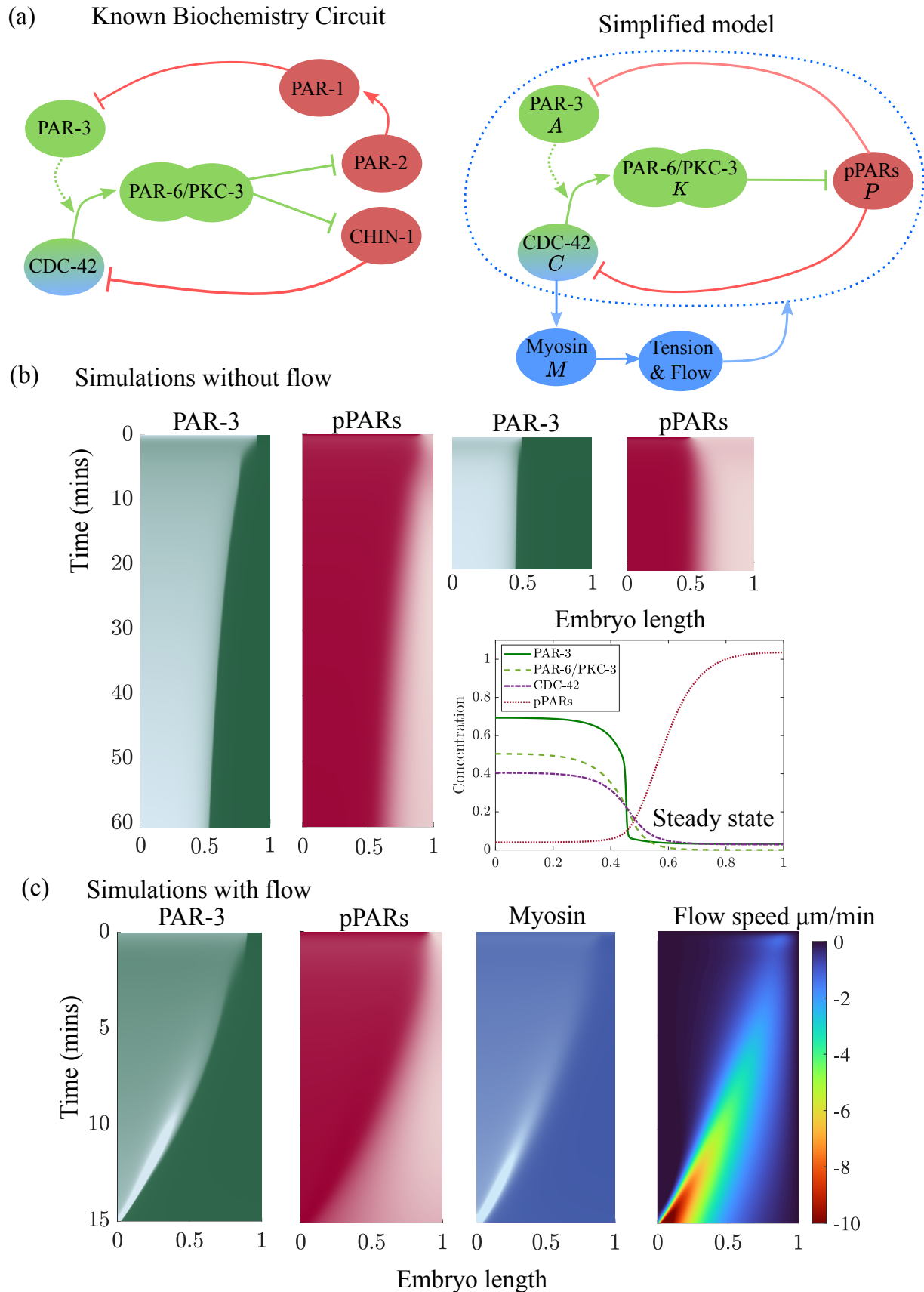
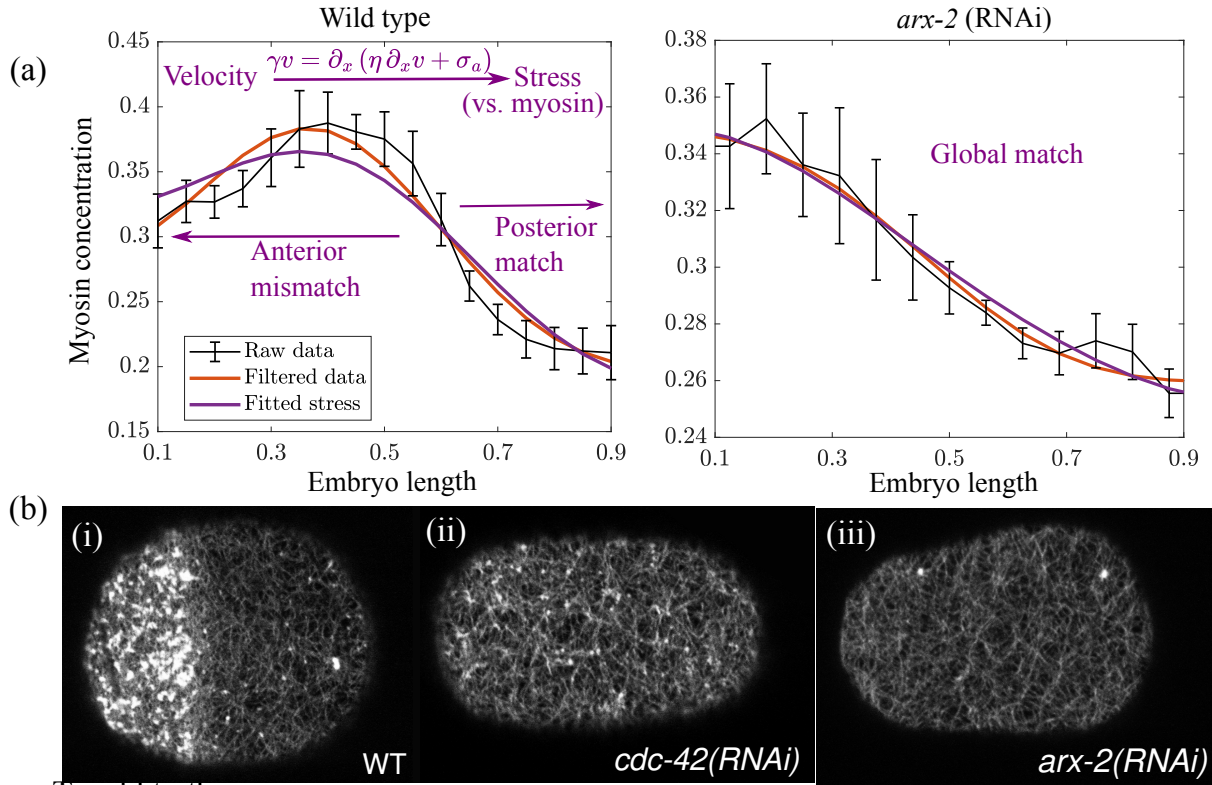


Figure 3: Models based a simple interaction of PAR proteins and myosin can stably maintain a polarity boundary, but cannot explain rescue. (a) Simplified model of PAR protein dynamics, and how it relates to the known system biochemistry (Lang and Munro, 2017). (b) Simulations without flow can maintain a stable boundary but cannot reproduce rescue in a realistic time. These panels show pseudo-kymographs of PAR-3 (green, left) and pPARs (red, right) in rescue (left, the boundary starts at 90% embryo length) and normal maintenance (right, the boundary starts at 50% embryo length) conditions. The bottom plot shows the unique steady state in the model without flow. (c) Simulations with flow lead to a vanishing anterior domain. Shown are pseudo-kymographs of the PAR-3, pPAR, and myosin concentrations over time, as well as the flow speeds. **First draft complete**



To add to this:

Branched actin phenotype with and without nocodazole
Pictures and kymographs

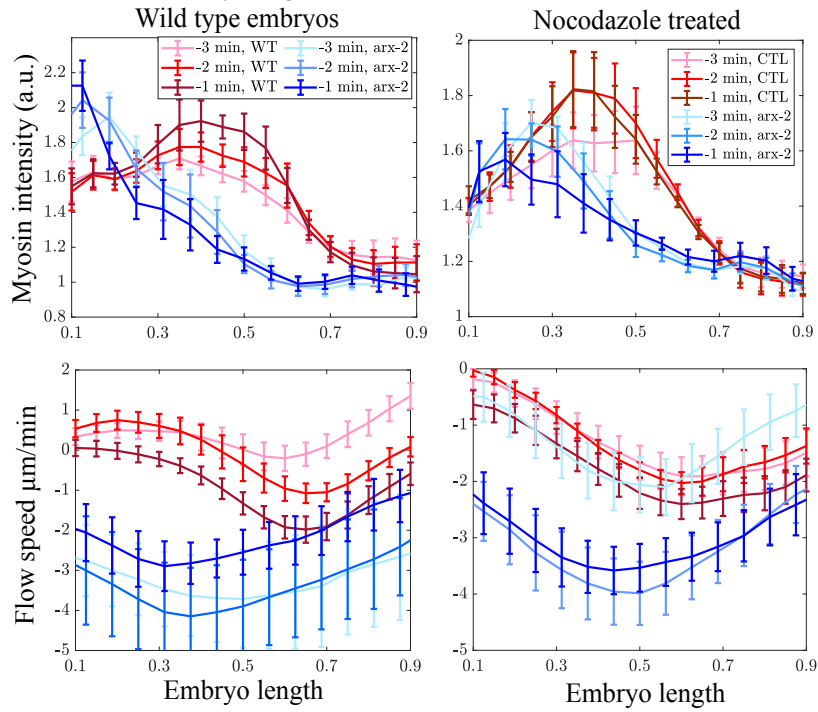


Figure 4: Branched actin acts in the anterior to suppress contractility in wild-type embryos.

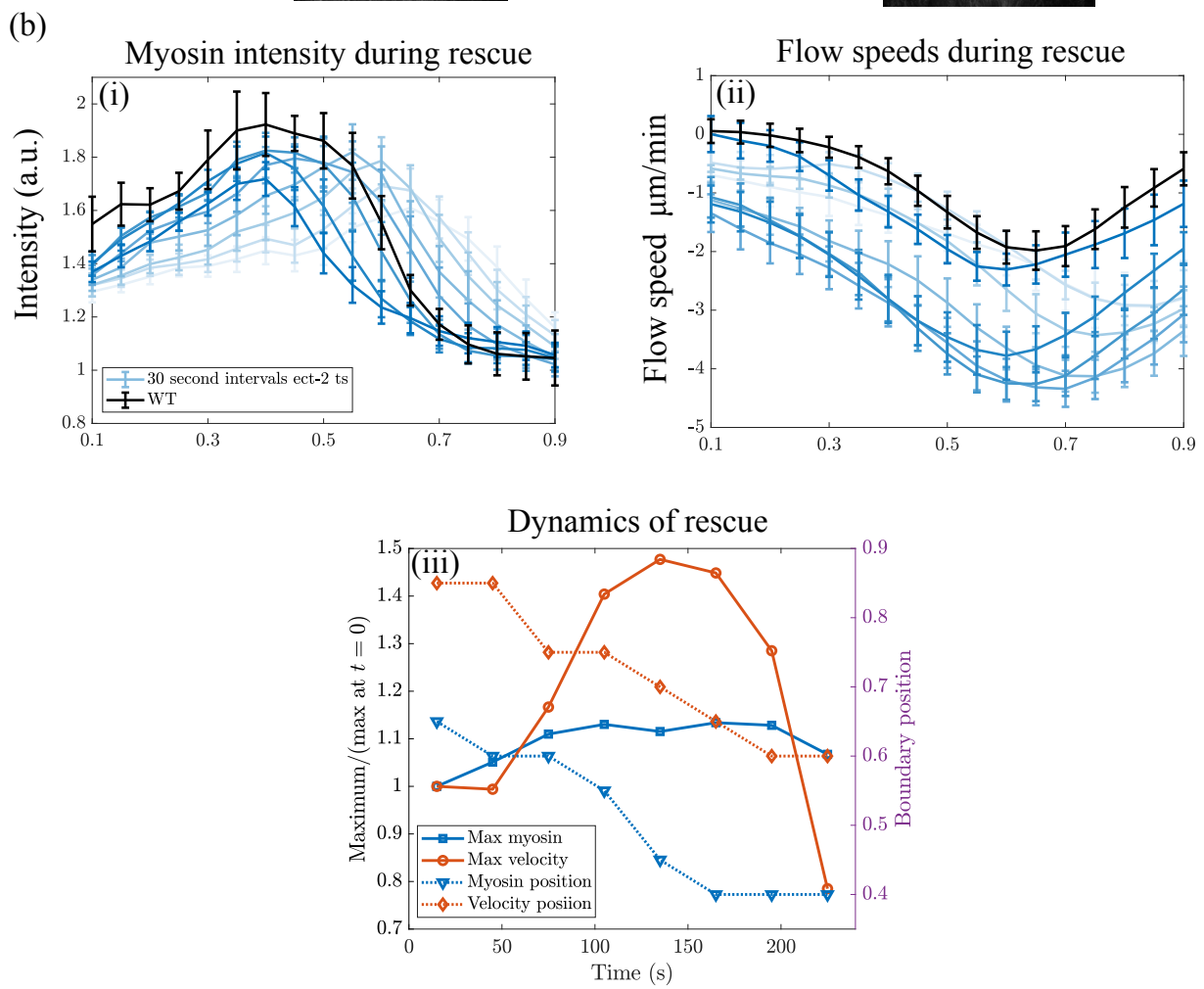
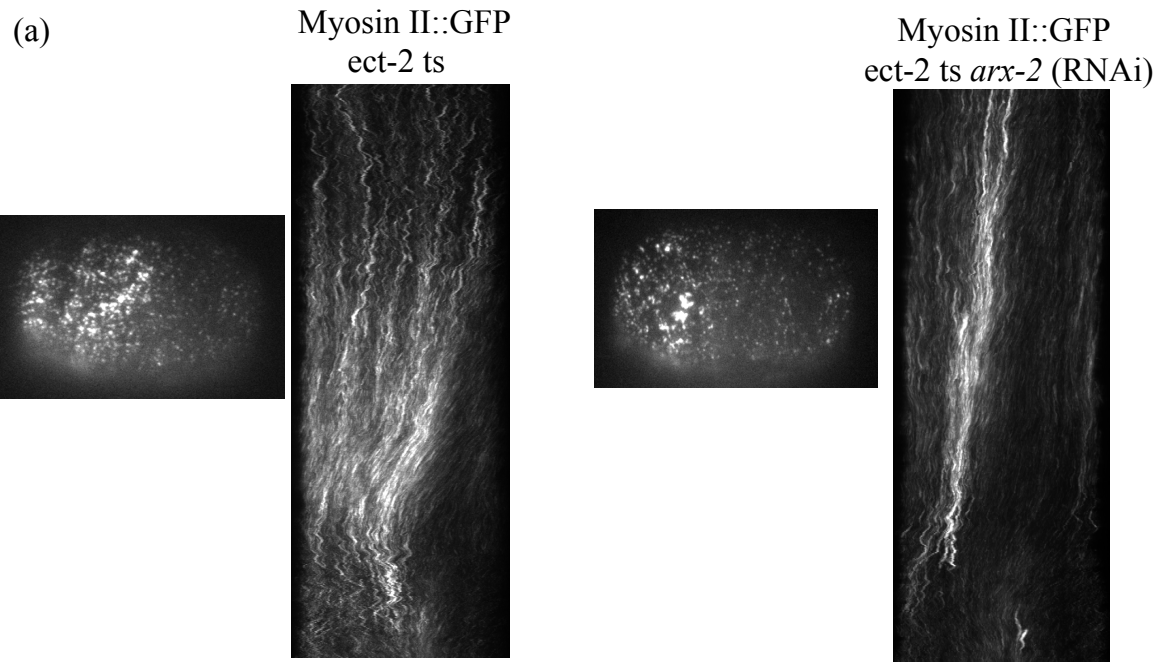
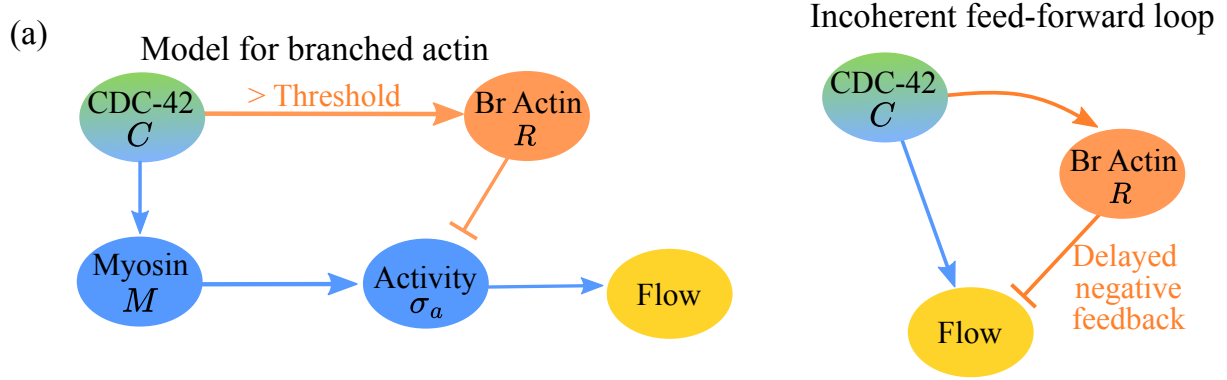


Figure 5: Branched actin acts suddenly to alleviate contractile tension in the anterior during maintenance phase rescue. (a) Still images and kymograph of myosin II (NMY-2::GFP) in ect-2 ts embryos (left) and ect-2 ts embryos with arx-2 (RNAi) (right). (b) Myosin intensity (i) and flow speeds (ii) in ect-2 (ts) embryos (blue lines) compared to wild-type. Data are shown at 30 second intervals using progressively darker lines, and wild-type data in the last minute of maintenance phase are shown in black. (c) Summary of rescue dynamics. Solid lines, governed by the left axis, show the maximum in myosin intensity (blue) and velocity (red), scaled by the value at the onset of maintenance phase ($t = 0$). Dashed lines, governed by the right axis, show the position of the peak in myosin (blue) and velocity (red) over time. **First draft complete.**



(b)

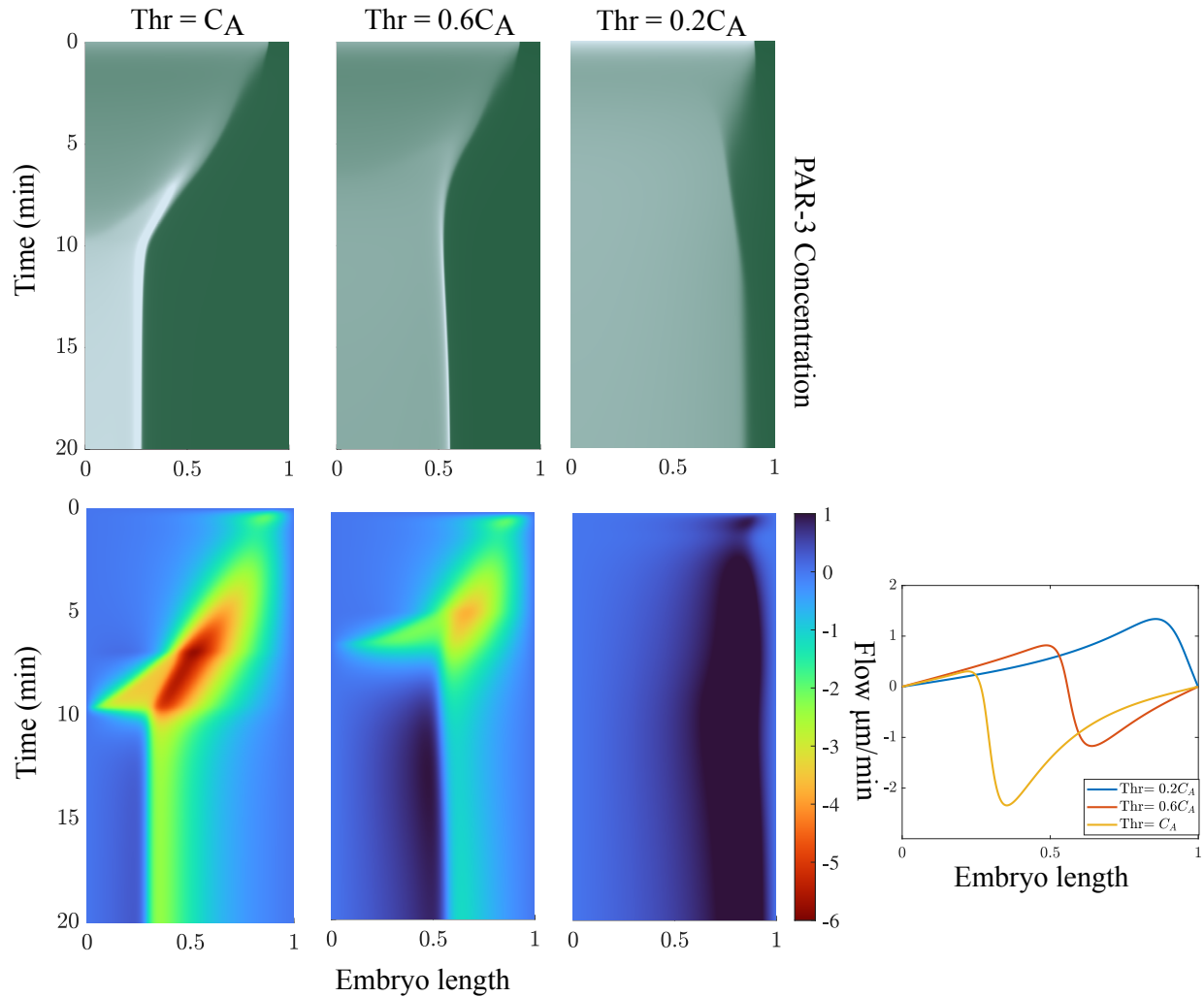


Figure 6: Models that incorporate branched actin successfully reproduce the dynamics of rescue. (a) Extension of the model presented in Fig. 3(a) to account for branched actin. Above a threshold of CDC-42, branched actin is produced and inhibits contractile stress. At its simplest level, these dynamics are an incoherent feed-forward loop (right). (b) Simulations with varying branched actin thresholds show varying degrees of contractility. Shown are kymographs of the PAR-3 domain (top) and flow speeds (bottom) over time. Each column shows a different threshold for branched actin, given in terms of the typical anterior CDC-42 concentration (0.4; see Fig. 3(b)). The steady state flow profiles for each threshold are also shown at bottom right. **First draft complete.**

References

- Donato Aceto, Melissa Beers, and Kenneth J Kemphues. Interaction of par-6 with cdc-42 is required for maintenance but not establishment of par asymmetry in *c. elegans*. *Developmental biology*, 299(2):386–397, 2006.
- Tom Bland, Nisha Hirani, David Briggs, Riccardo Rossetto, KangBo Ng, Neil Q McDonald, David Zwicker, and Nathan W Goehring. Optimized dimerization of the par-2 ring domain drives cooperative and selective membrane recruitment for robust feedback-driven cell polarization. *bioRxiv*, pages 2023–08, 2023.
- Justin S Bois, Frank Jülicher, and Stephan W Grill. Pattern formation in active fluids. *Biophysical Journal*, 100(3):445a, 2011.
- Carrie R Cowan and Anthony A Hyman. Acto-myosin reorganization and par polarity in *c. elegans*. 2007.
- Adrian A Cuenca, Aaron Schetter, Donato Aceto, Kenneth Kemphues, and Geraldine Seydoux. Polarization of the *c. elegans* zygote proceeds via distinct establishment and maintenance phases. 2003.
- Adriana T Dawes and Edwin M Munro. Par-3 oligomerization may provide an actin-independent mechanism to maintain distinct par protein domains in the early *caenorhabditis elegans* embryo. *Biophysical journal*, 101(6):1412–1422, 2011.
- Evan B Dewey, Danielle T Taylor, and Christopher A Johnston. Cell fate decision making through oriented cell division. *Journal of developmental biology*, 3(4):129–157, 2015.

Nathan W Goehring, Philipp Khuc Trong, Justin S Bois, Debanjan Chowdhury, Ernesto M Nicola, Anthony A Hyman, and Stephan W Grill. Polarization of par proteins by advective triggering of a pattern-forming system. *Science*, 334(6059):1137–1141, 2011.

Bob Goldstein and Ian G Macara. The par proteins: fundamental players in animal cell polarization. *Developmental cell*, 13(5):609–622, 2007.

Monica Gotta, Mary C Abraham, and Julie Ahringer. Cdc-42 controls early cell polarity and spindle orientation in *c. elegans*. *Current biology*, 11(7):482–488, 2001.

Peter Gross, K Vijay Kumar, Nathan W Goehring, Justin S Bois, Carsten Hoege, Frank Jülicher, and Stephan W Grill. Guiding self-organized pattern formation in cell polarity establishment. *Nature physics*, 15(3):293–300, 2019.

Niv Ierushalmi and Kinneret Keren. Cytoskeletal symmetry breaking in animal cells. *Current Opinion in Cell Biology*, 72:91–99, 2021.

Rukshala Illukkumbura, Nisha Hirani, Joana Borrego-Pinto, Tom Bland, KangBo Ng, Lars Hübatsch, Jessica McQuade, Robert G Endres, and Nathan W Goehring. Design principles for selective polarization of par proteins by cortical flows. *Journal of Cell Biology*, 222(8), 2023.

Sukriti Kapoor and Sachin Kotak. Centrosome aurora a regulates rhogef ect-2 localisation and ensures a single par-2 polarity axis in *c. elegans* embryos. *Development*, 146(22):dev174565, 2019.

Amanda J Kay and Craig P Hunter. Cdc-42 regulates par protein localization and function to control cellular and embryonic polarity in *c. elegans*. *Current Biology*, 11(7):474–481, 2001.

Kraig T Kumfer, Steven J Cook, Jayne M Squirrell, Kevin W Eliceiri, Nina Peel, Kevin F O’Connell, and John G White. Cgef-1 and chin-1 regulate cdc-42 activity during asymmetric division in the *caenorhabditis elegans* embryo. *Molecular biology of the cell*, 21(2):266–277, 2010.

Charles F Lang and Edwin Munro. The par proteins: from molecular circuits to dynamic self-stabilizing cell polarity. *Development*, 144(19):3405–3416, 2017.

Charles F Lang, Alexander Anneken, and Edwin Munro. Oligomerization and feedback on membrane recruitment stabilize par-3 asymmetries in *c. elegans* zygotes. *bioRxiv*, pages 2023–08, 2023.

Rong Li and Bruce Bowerman. Symmetry breaking in biology. *Cold Spring Harbor perspectives in biology*, 2(3):a003475, 2010.

Katrina M Longhini and Michael Glotzer. Aurora a and cortical flows promote polarization and cytokinesis by inducing asymmetric ect-2 accumulation. *Elife*, 11:e83992, 2022.

Jean-Léon Maître, Hervé Turlier, Rukshala Illukkumbura, Björn Eismann, Ritsuya Niwayama, François Nédélec, and Takashi Hiiragi. Asymmetric division of contractile domains couples cell positioning and fate specification. *Nature*, 536(7616):344–348, 2016.

Mirjam Mayer, Martin Depken, Justin S Bois, Frank Jülicher, and Stephan W Grill. Anisotropies in cortical tension reveal the physical basis of polarizing cortical flows. *Nature*, 467(7315):617–621, 2010.

Ani Michaud, Marcin Leda, Zachary T Swider, Songeun Kim, Jiaye He, Jennifer Landino, Jenna R Valley, Jan Huisken, Andrew B Goryachev, George von Dassow, et al. A versatile cortical pattern-forming circuit based on rho, f-actin, ect2, and rga-3/4. *Journal of Cell Biology*, 221(8):e202203017, 2022.

Jonathan B Michaux, François B Robin, William M McFadden, and Edwin M Munro. Excitable rhoa dynamics drive pulsed contractions in the early *c. elegans* embryo. *Journal of Cell Biology*, 217(12):4230–4252, 2018.

Yoichiro Mori, Alexandra Jilkine, and Leah Edelstein-Keshet. Wave-pinning and cell polarity from a bistable reaction-diffusion system. *Biophysical journal*, 94(9):3684–3697, 2008.

Fumio Motegi and Asako Sugimoto. Sequential functioning of the ect-2 rhogef, rho-1 and cdc-42 establishes cell polarity in *caenorhabditis elegans* embryos. *Nature cell biology*, 8(9):978–985, 2006.

Fumio Motegi, Seth Zonies, Yingsong Hao, Adrian A Cuenca, Erik Griffin, and Geraldine Seydoux. Microtubules induce self-organization of polarized par domains in *caenorhabditis elegans* zygotes. *Nature cell biology*, 13(11):1361–1367, 2011.

Edwin Munro and Bruce Bowerman. Cellular symmetry breaking during *caenorhabditis elegans* development. *Cold Spring Harbor perspectives in biology*, 1(4):a003400, 2009.

Edwin Munro, Jeremy Nance, and James R Priess. Cortical flows powered by asymmetrical contraction transport par proteins to establish and maintain anterior-posterior polarity in the early *c. elegans* embryo. *Developmental cell*, 7(3):413–424, 2004.

Camelia G Muresan, Zachary Gao Sun, Vikrant Yadav, A Pasha Tabatabai, Laura Lanier, June Hyung Kim, Taeyoon Kim, and Michael P Murrell. F-actin architecture determines constraints on myosin thick filament motion. *Nature communications*, 13(1):7008, 2022.

Masatoshi Nishikawa, Sundar Ram Naganathan, Frank Jülicher, and Stephan W Grill. Controlling contractile instabilities in the actomyosin cortex. *Elife*, 6:e19595, 2017.

Alice Y Pollitt and Robert H Insall. Wasp and scar/wave proteins: the drivers of actin assembly. *Journal of cell science*, 122(15):2575–2578, 2009.

François B Robin, William M McFadden, Baixue Yao, and Edwin M Munro. Single-molecule analysis of cell surface dynamics in *caenorhabditis elegans* embryos. *Nature methods*, 11(6):677–682, 2014.

Josana Rodriguez, Florent Peglion, Jack Martin, Lars Hubatsch, Jacob Reich, Nisha Hirani, Alicia G Gubieda, Jon Roffey, Artur Ribeiro Fernandes, Daniel St Johnston, et al. apkc cycles between functionally distinct par protein assemblies to drive cell polarity. *Developmental cell*, 42(4):400–415, 2017.

Anne Sailer, Alexander Anneken, Younan Li, Sam Lee, and Edwin Munro. Dynamic opposition of clustered proteins stabilizes cortical polarity in the *c. elegans* zygote. *Developmental cell*, 35(1):131–142, 2015.

Stephanie Schonegg and Anthony A Hyman. Cdc-42 and rho-1 coordinate acto-myosin contractility and par protein localization during polarity establishment in *c. elegans* embryos. 2006.

Yu Chung Tse, Michael Werner, Katrina M Longhini, Jean-Claude Labbe, Bob Goldstein, and Michael Glotzer. Rhoa activation during polarization and cytokinesis of the early *caenorhabditis elegans* embryo is differentially dependent on nop-1 and cyk-4. *Molecular biology of the cell*, 23(20):4020–4031, 2012.

Qing Yang, Xiao-Feng Zhang, Thomas D Pollard, and Paul Forscher. Arp2/3 complex-dependent actin networks constrain myosin ii function in driving retrograde actin flow. *Journal of Cell Biology*, 197(7):939–956, 2012.

Baixue Yao, Seth Donoughe, Jonathan Michaux, and Edwin Munro. Modulating rhoa effectors induces transitions to oscillatory and more wavelike rhoa dynamics in *caenorhabditis elegans* zygotes. *Molecular Biology of the Cell*, 33(6):ar58, 2022.

Seth Zonies, Fumio Motegi, Yingsong Hao, and Geraldine Seydoux. Symmetry breaking and polarization of the *c. elegans* zygote by the polarity protein par-2. *Development*, 137(10):1669–1677, 2010.